Decay of Interface Correlation in Thin Polymer Films

P. Müller-Buschbaum,*,† J. S. Gutmann,†,‡ C. Lorenz,† T. Schmitt,† and M. Stamm†

Max-Planck-Institut für Polymerforschung, Ackermannweg 10, 55128 Mainz, Germany, and Institut TMC, Universität Hamburg, Bundesstrasse 45, 20146 Hamburg, Germany

Received August 19, 1998; Revised Manuscript Received October 17, 1998

ABSTRACT: The long-range interface correlation in thin polymer films (polystyrene and fully brominated polystyrene) prepared by spin-coating is examined. Using diffuse X-ray scattering at small angles of incidence, the roughness correlation which dominates the surface morphology of the polymer film is probed from mesoscopic down to molecular in-plane distances. At the smallest replicable in-plane length scale, the crossover from a conformal to a statistically independent roughness spectrum is determined. The influences of molecular weight and film thickness are discussed. Compared to annealed samples, the as-prepared ones show a different scaling behavior, which is explained with simple models taking surface-bending rigidity into account. With a real-time annealing investigation, the decay of interface correlation after the onset of annealing has been followed. At annealing even below the glass-transition temperature, the roughness correlation is changing and disappears during sufficiently long annealing in the melt. Monitoring the changes with time probes the mobility of the polymer molecules at the polymer−vacuum interface. In thin films, the time constant is increased. The determined surface diffusion coefficient shows a slowing down as compared to the bulk behavior which may be attributed to the attractive, long-range substrate−interface interaction.

Introduction

Spin-coating is a widely used technique for the preparation of thin polymer films on top of solid substrates. Depending on the used polymer/solvent combination, films with a very uniform thickness and small surface roughness can be obtained. Controlled by the preparation parameters, film thicknesses in a wide range from the submonolayer regime up to several microns may be prepared. Due to the importance of technical applications such as protective coatings in microelectronics and optics, previous publications determine approximations which enable the calculation of the resulting film thickness as a function of polymer concentration, viscosity, molecular weight, and spinning parameters.[1−3] However, due to the complex nature of the spin-coating process major simplifying assumptions have been used, and thus, the successful modeling is restricted to a few homopolymer systems. Less attention was paid to the resulting surface morphology of the thin polymer films directly after preparation. In a recent publication,[4] a roughness correlation between the substrate and the polymer surface was observed. In a wide film thickness range above the entanglement molecular weight, the polymer surface is determined by the substrate morphology. Only after annealing well above the glass-transition temperature is this long-range correlation imposed by the spin-coating lost. Consequently, the smallest achievable surface roughness is determined by the substrate roughness in systems where annealing is not possible.

While in the previous experiments[4] the influence of several preparation and polymer parameters on the installation of correlated roughness was determined, in the present investigation, the range of the replicated roughness spectrum as well as the time-dependent decay of the long-range correlation is addressed. We examine several film thicknesses of polystyrene (PS) and fully brominated polystyrene (PBrS) at fixed molecular weight and examine for PS additionally the influence of molecular weight. With diffuse X-ray scattering, the surface morphology, the correlation between interfaces, and the decay of long-range correlation were measured. The experimentally determined film thickness dependence of the short-wavelength cutoff of the replicated roughness is discussed within two simple models, which explain the different scaling behavior between untreated and annealed samples. During annealing studies, the decay of long-range correlation is followed in situ. These measurements probe the mobility of the polymer chains at the polymer−vacuum interface. The determined surface diffusion constant shows the slowing down of diffusion near an attractive wall.

In this paper, the Introduction is followed by the Experimental Section describing the sample preparation. The next section shortly introduces some aspects of diffuse scattering, and X-ray measurements are reported. The results and discussion conclude the paper.

Experimental Section

Sample Preparation. Si(100) surfaces covered with a native oxide layer were treated in several cleaning cycles, always by four different baths (deionized water, 2-propanol, acetone, and toluene), before being used as substrates. Immediately before coating, the dry wafers were flushed with fresh toluene once again. Next, the thin films were prepared by spin-coating (1950 rpm for 30 s) by depositing a toluene solution of the polymer onto the wafer. We used polystyrene (PS) with molecular weights (M_w) of 28, 31, 67, 106, and 672 kg/mol and brominated polystyrene (PBrS) with M_w = 144.7 kg/mol (before bromination) and a degree of bromination of x = 1.07. All used polymers have a narrow molecular weight distribution $M_w/M_n \leq 1.05$. The film thickness was varied by changing the concentration of the solution following an empirical relation.[3]

With X-ray reflectivity, the initial film thicknesses of the polymer films were determined. All diffuse X-ray scattering

* To whom correspondence should be addressed.
† Max-Planck-Institut für Polymerforschung.
‡ Institut TMC, Universität Hamburg.

10.1021/ma981311l CCC: $15.00
Published on Web 12/09/1998

experiments were performed in a vacuum sample cell. Its thermoelectric heating and the horizontally placed sample enable an in situ annealing of the samples during X-ray scans. Thus, real-time experiments were possible. The annealing studies were restricted to the PBrS films, because the PS films exhibit dewetting.[4] The annealing of PBrS was performed at three different temperatures, $T_1 = 122.8$ °C (below the glass-transition temperature $T_g = 134$ °C as determined by DSC), $T_2 = 161.3$ °C (above T_g), and $T_3 = 191.2$ °C (significantly above T_g). Only at T_3 was an equilibrium state reached within typical time scales that can be reached in synchrotron in situ experiments (beam time is limited to a few days only). Annealing was stopped after no changes in the X-ray scans were visible over a sufficiently large time (typically twice the previous annealing time), e.g., after 8 h. Next, the sample was quenched down to room temperature and remeasured.

Diffuse X-ray Scattering. Diffuse X-ray scattering probes the in-plane wave vector dependence of the long-wavelength fluctuations.[5] This enables the determination of the displacement−displacement correlation function without assumptions about the local layer structure. Correlations between the interfaces yield a coupling of the correlation functions of the individual interfaces. These interfaces are, in our case, the air−polymer and polymer−substrate interfaces. With off-specular scans, direct information about such an interface correlation is obtained.[6] In the case of uncorrelated interfaces, all interfaces scatter independently and the diffuse intensities of all individual interfaces superpose. Partially or fully correlated roughness gives rise to scattering with partial coherence, and resonant diffuse scattering (RDS) is observed. The partial phase coherence of the waves diffusely scattered from different interfaces concentrates the intensity in narrow sheets. These sheets of resonant diffuse scattering are oriented parallel to the q_x axis with the center fulfilling the one-dimensional Bragg condition[7] $\Delta q_z = 2\pi/d^{\mathrm{corr}}$. The modulations of the resonant diffuse scattering are in-phase with the fringes of the reflectivity and display the distance (d^{corr}) of the correlated interfaces. Due to the angle-dependent refraction of the X-rays in a q_xq_z map, the sheets are curved, forming the so-called "RDS bananas".[7]

The sample surface defines the *xy* plane, and the scattering vector is denoted by $\vec{q} = (q_x, q_y, q_z)$. Within a *m*-layer system, the *z* component of the momentum transfer in each layer is given by $q_{0,j} = k_{(z,i),j} + k_{(z,f),j}$, $q_{1,j} = k_{(z,i),j} - k_{(z,f),j}$, $q_{2,j} = -q_{1,j}$, and $q_{3,j} = -q_{0,j}$, introducing the *z* components $k_{(z,i),j}$ and $k_{(z,f),j}$ of the incident and diffracted wave vectors in medium *j*, respectively. The *j*th layer is described by the refractive index (n_j), the rms roughness (σ_j), and the displacement−displacement autocorrelation function ($C_{j,j}(X)$). Within the distorted-wave Born approximation (DWBA), the diffuse scattering cross section[7] is given by

$$\left(\frac{\mathrm{d}\sigma}{\mathrm{d}\Omega}\right)_{\mathrm{diff}} = \frac{F\,\pi^2}{\lambda^4}\sum_{j,k=1}^{m}(n_j^{\,2} - n_{j+1}^{\,2})(n_k^{\,2} - n_{k+1}^{\,2})^*\sum_{h,l=0}^{3} G_{h,j}G_{l,k}^*\,S_{j,k}^{h,l} \tag{1}$$

with

$$S_{j,k}^{h,l} = \exp\{-0.5[q_{h,j}^{\,2}\sigma_j^{\,2} + q_{l,k}^{*\,2}\sigma_k^{\,2}] - i[q_{h,j}z_j + q_{l,k}^*z_k]\} \times (q_{h,j}q_{l,k}^*)^{-1}\int_0^\infty \mathrm{d}X\,(\exp\{q_{h,j}q_{l,k}^*C_{j,k}(X)\} - 1)\cos(q_xX) \tag{2}$$

The prefactors $G_{k,j}$ are defined as $G_{0,j} = T_{i,j}T_{f,j}$, $G_{1,j} = T_{i,j}R_{f,j}$, $G_{2,j} = R_{i,j}T_{f,j}$, and $G_{3,j} = R_{i,j}R_{f,j}$, with the amplitudes of the transmitted waves $T_{i,j}$ and $T_{f,j}$ and the reflected waves $R_{i,j}$ and $R_{f,j}$ within the *j*th layer. These amplitudes can easily be calculated using standard recurrence relations.[8−10] The illuminated area of the sample is denoted by *F*. As it can be seen from eq 2, the phases of the scattering contributions of the different interfaces *j* and *k* differ. Therefore, the summand (*j*,*k*) of the double sum includes a phase factor. In the case of correlated roughness, these summands (*j*,*k*) and the symmetric counterparts (*k*,*j*) contribute to the diffuse scattering. Due to the constructive interference of the diffusely scattered beams, sheets of enhanced intensity are created at a distance of $2\pi/(z_j - z_k)$.

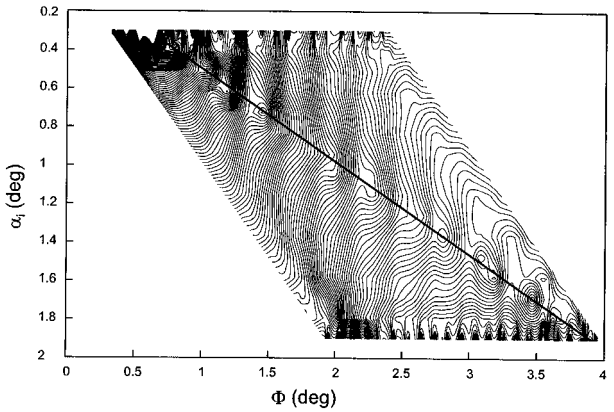

Figure 1. Contour plot of the scattered intensity distribution with a logarithmic contour line spacing. The incident angle is denoted with α_i and the detector angle with $\phi = \alpha_i + \alpha_f$. Due to the inaccessible area (behind the sample) and the fixed scan range of each detector scan, the contour area becomes a trapezoidal shape. The thick solid line fulfilling $\Phi = 2\alpha_i$ represents the specular streak (reflectivity). Narrowed contour lines show an increased intensity.

Due to the different angular dependence of the maxima in a "detector scan" in systems consisting of one single layer on top of a semiinfinite substrate, an easy separation of maxima which are caused by the roughness correlation from maxima that are caused by dynamical effects is possible. Thus, one single detector scan is sufficient to give evidence of vertical replication of roughness.

X-ray Measurements. One typical path through the reciprocal space is called a detector scan: The sample is held fixed at one angle of incidence (α_i), and the detector position is varied around the specular peak. According to $\Delta q_x \sim \pm(2\pi/\lambda)\alpha\Delta\alpha$ and $\Delta q_z \sim (2\pi/\lambda)\Delta\alpha$, the changes in the exit angle ($\Delta\alpha$) will mainly result in a change of q_z and only very small changes in q_x. In a q_xq_z map, a detector scan is a parabolic path through the reciprocal space, which cuts the Yoneda[11] as well as the specular streak. In a scan, both are visible as peaks. The intensity depends on the roughness of the sample and the chosen incident angle (α_i). In the case of correlated roughness, one observes intensity streaks of resonant diffuse scattering that are oriented parallel to the q_x axis. This yields a modulation of the intensity in a detector scan as pointed out in the previous section,[12] and from the spacing of the fringes $\Delta q_z = 2\pi/d^{\mathrm{corr}}$, the distance between the correlated interfaces (d^{corr}) can be estimated. Performing several detector scans at different angles of incidence yields a mapping of a part of the reciprocal space. This is shown in real space in a contour line picture with a logarithmic spacing of the contour lines in Figure 1. The specular streak is pictured by the thick solid line fulfilling the condition $\Phi = 2\alpha_i$ (reflectivity). The resonant diffuse scattering is visible as the black-shaded areas oriented parallel to the α_i axis and the Yoneda streak by the increased intensity, fulfilling $\Phi = \alpha_i + \alpha_c$.

X-ray reflectivity measurements and a mapping consisting of several detector scans of the homogeneous films directly after preparation without any further treatment were performed at a laboratory X-ray source ($\lambda = 1.54$ Å). The Θ−Θ reflectometer (Seifert XRD 3003TT) enables a large dynamic range of 8 orders of magnitude in intensity and is therefore well suited for diffuse measurements. As the monochromator, a Ge(110) channel cut crystal is used. The sample is placed on a specially designed vacuum chuck and is measured under air. The reflectivity curves of the homogeneous PS films exhibit well-pronounced fringes due to the small surface roughness of typically 5 Å. From a fit of the reflectivity data, the film thicknesses of the as-prepared samples (l_{tot}) were obtained. The mapping (see Figure 1) shows sheets of enhanced intensity

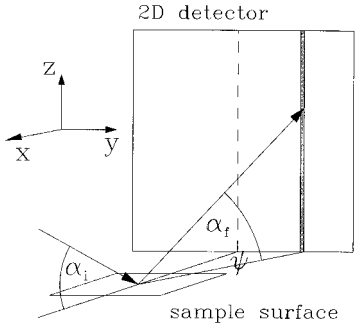

Figure 2. Schematic drawing of the experimental setup used in the scattering experiment utilizing the 2D detector. The sample surface is horizontally placed. The angle of incidence is denoted with α_i, the exit angle with α_f, and the out-of plane angle with Ψ. For data evaluation, several vertical slices are taken. The *xy* plane denotes the sample surface.

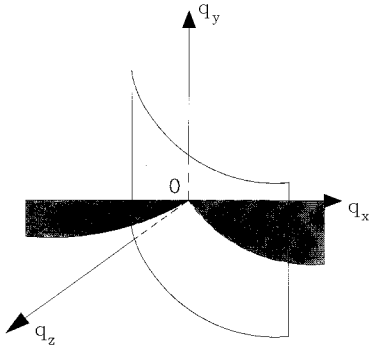

Figure 3. Schematic drawing of the reciprocal space. In the frequently plotted q_xq_z plane, only the inaccessible range (dark gray planes) and the parabolic path of a detector scan (solid line) are shown. A reflectivity scan will follow the q_z axis with $q_x = q_y = 0$. The light gray parabolic curved plane pictures off-detector scans with increasing q_y component.

oriented parallel to the α_i axis which are in-phase with the fringes of the reflectivity (seen in the diagonal) due to resonant diffuse scattering. Consequently, we detect a roughness correlation between the substrate surface and the polymer surface. To obtain information about the range of the roughness spectrum which is replicated by the thin polymer film, additional diffuse scans are necessary.

These diffuse X-ray measurements were performed at the BW4 USAX beamline of the DORIS III storage ring at HASYLAB/DESY in Hamburg. The selected wavelength was $\lambda = 1.38$ Å. We employed a reflection geometry[13] to realize the diffuse X-ray scattering under the conditions of small-angle scattering with a setup of high-quality entrance slits and a completely evacuated pathway. Details concerning the beamline, which is normally used for ultra-small-angle scattering in transmission geometry, are reported in ref 14. To picture the geometry used in this experiment, a schematical drawing of the setup is shown in Figure 2. The beam divergence in and out of the plane of reflection was set by two entrance cross-slits. At an incident angle of $\alpha_i = 0.98°$, the coherently illuminated length on the sample surface is $\xi_{surf} \cong 500$ μm, and perpendicular to the surface, the coherence length is $\xi_{hor} \cong 8$ μm.[15] At a sample−detector distance of 2903 mm, a resolution of approximately 6.1×10^{-4} Å^{-1} was achieved. A beam stop in front of the detector was installed at the position of the primary beam. The nonspecular as well as the specular intensity was recorded with a two-dimensional gas detector consisting of a 512 × 512 pixel array.[16] At one fixed angle of incidence, the two-dimensional intensity distribution consists of several vertical and horizontal slices. A vertical slice at $q_y = 0$ Å^{-1} correspond to a detector scan, and horizontal slices correspond to so-called out-of plane scans.[17] Vertical slices at $q_y \neq 0$ Å^{-1} are called "off-detector scans". These scans are paths through the reciprocal space shifted parallel to the parabolic path of a detector scan due to the additional q_y component. Figure 3 illustrates this. In the q_xq_z plane, the inaccessible areas (dark gray planes) and a detector scan (solid line in the q_xq_z plane) are shown. The light gray plane with a parabolic curvature shows the part of $q_xq_yq_z$ mapping that is accessible with off-detector scans. The disappearance of the interference fringes in the off-detector scans with increasing q_y value indicates that the top and bottom interfaces of the polymer film are no longer correlated. Thus, the smallest replicated in-plane length scale (R_c) can be estimated by successively measuring off-detector scans with increasing q_y. In our setup, this is equivalent to several vertical cuts of the two-dimensional intensity with increasing q_y.

Results and Discussion

The replication of a part of the roughness spectrum from one interface by another interface yields a correlation between both. The resulting in-plane morphology of the upper layer then strongly depends on the underlying one. The case of a one-layer system can be pictured by a thin layer of snow on a hilly ground. The snow layer follows the curvature of the ground. In two-layer or multilayer systems, the degree of freedom concerning the number of replicated interfaces and the transferred roughness spectrum is enlarged. In the literature, interface correlation was observed not only for thin polymer films but also for thin solid films,[18−22] Langmuir−Blodgett films,[23,24] and smectic films.[25,26]

Static Measurements. The diffuse scattering measurements were performed at an angle of incidence $\alpha_i > \alpha_c$, i.e., above the critical angle of total reflection of the polymer film. Therefore, typical characteristics (Yoneda peak, specular peak, modulations due to resonant diffuse scattering) can be easily separated on the two-dimensional detector array. Cuts along the direction of a detector scan are shown in Figure 4 as an example of thin films of brominated polystyrene. $\Phi = \alpha_i + \alpha_f$ denotes the detector angle. In the horizontal direction, the intensity was integrated over $\Delta q_y = \pm 9.1 \times 10^{-4}$ Å^{-1}. The Yoneda peak is observed at $\Phi = 1.17°$ and the specular peak at $\Phi = 1.99°$. Additional modulations of the intensity originate from resonant diffuse scattering. In Figure 4, the thickness of the PBrS film is varied between $l_{tot} = 292$ and 659 Å at a constant molecular weight. The bare Si substrate (denoted "without") is shown for comparison. All samples exhibit correlated roughness.

As discussed above, to probe the range of correlated in-plane length scales, cuts with an increasing q_y component have to be performed.[26] Figure 5 shows these off-detector scans for PBrS and a film thickness of $l_{tot} = 292$ Å. From the bottom to the top, q_y increases in steps of $\Delta q_y = 6.1 \times 10^{-4}$ Å^{-1}. The curves are shifted against each other for clarity. The decreasing amplitude of the fringes resulting from resonant diffuse scattering with increasing q_y indicates the loss of correlation at smaller in-plane length scales. At long in-plane length scales, the substrate and the polymer−vacuum interface are highly correlated. The conformality between the bottom and the top of the polymer layer vanishes at decreasing in-plane length scales. Taking the roughness spectrum of the underlying substrate as a distortion of the polymer surface, one can define a characteristic decay length of this distortion, yielding a cutoff in-plane length scale (R_c). Thus, the substrate morphology is replicated by the thin polymer film for in-plane length scales $R > R_c$. Figure 6 pictures this (for clarity, the

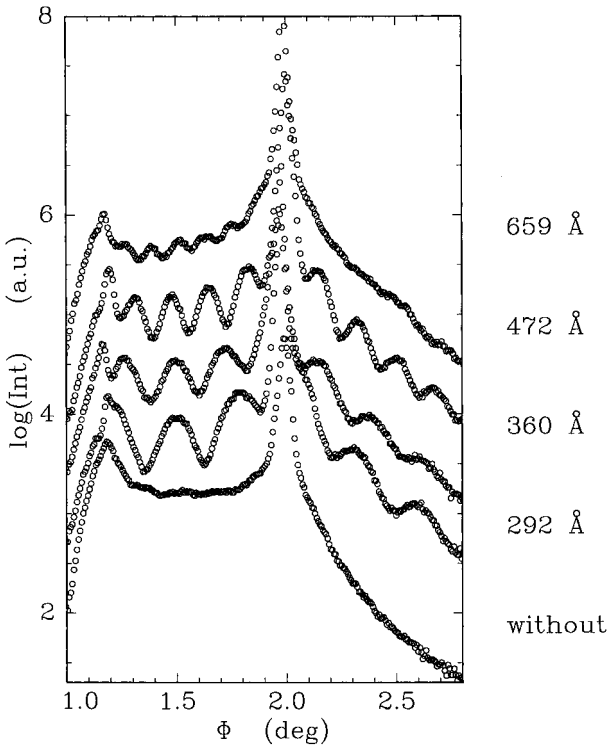

Figure 4. Detector scans measured at the angle of incidence $\alpha_i = 0.99°$ of the PBrS films as prepared for different film thicknesses l_{tot}. For clarity, the curves are shifted against each other. For comparison, the data obtained from the bare silicon wafer are shown, too (without).

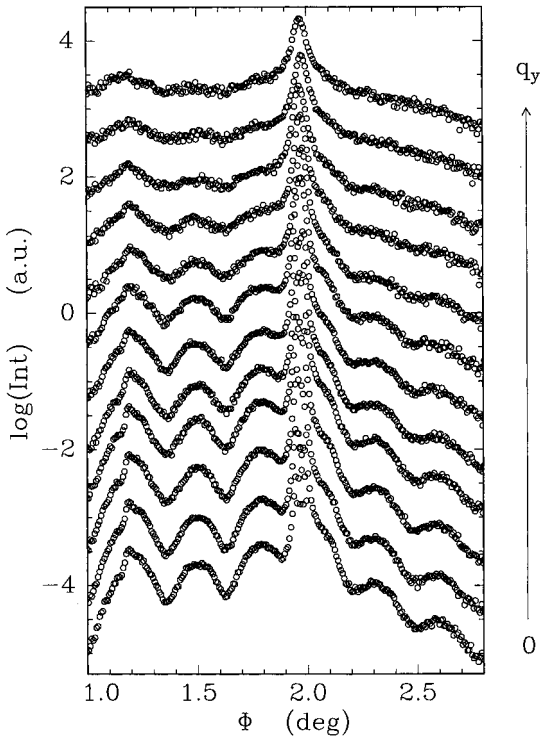

Figure 5. Off-detector scans measured at the angle of incidence $\alpha_i = 0.98°$ for a PBrS film with a film thickness of $l_{tot} = 292$ Å at different values of q_y showing the disappearance of interference fringes of the resonant diffuse scattering. The increase in q_y from the bottom to the top is shown with the arrow. For clarity, the curves are shifted against each other.

roughness amplitude is strongly enlarged against the film thickness l_{tot}).

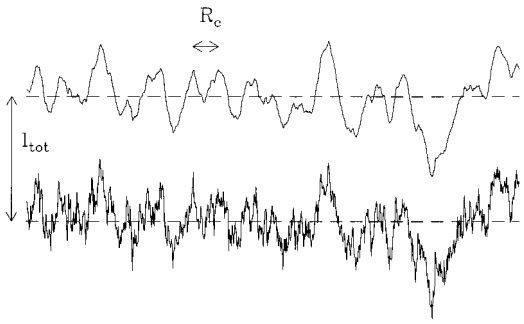

Figure 6. Schematic drawing of two interfaces at a mean distance l_{tot}, corresponding to the film thickness as obtained from reflectivity experiments (mean interface position marked with the dashed lines). The roughness spectrum of the lower interface is only transferred for in-plane length scales bigger than R_c. The amplitude of the roughness is greatly exaggerated for clarity.

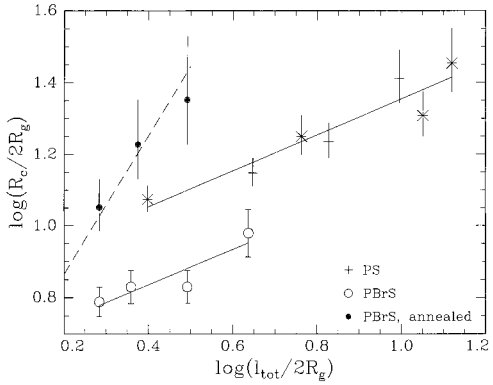

Figure 7. Double-logarithmic plot of the smallest replicated in-plane length scale R_c normalized by the radius of gyration R_g as a function of the total film thickness after preparation l_{tot}. The data obtained from samples right after preparation are shown with crosses (PS, 28K), stars (PS, 67K), and open circles (PBrS). Data from the samples in the melt state are shown with filled circles (PBrS). The solid and dashed lines are fits to the data yielding a scaling behavior based on models as explained in the text.

As a function of the molecular weight of the PS films, we do not observe changes of this short-wavelength cutoff $q_c = 2\pi/R_c$ in the examined molecular weight range of 28−672 kg/mol (which are above the entanglement molecular weight[27]). Thus, we discuss only the dependence of R_c on l_{tot}. To relate the results to typical polymer dimensions, both lengths, l_{tot} and R_c, are normalized by the radius of gyration (R_g) of the unperturbed chains. In a double-logarithmic plot, these results are presented in Figure 7. It shows a combined plot of measurements from unannealed PBrS samples (open circles) and PS samples of two different molecular weights (28K, crosses, and 67K, stars) as well as annealed PBrS samples (solid circles). The error bars result from the resolution of our setup and the limited statistics of off-detector scans. Both types of PS and PBrS samples exhibit the same scaling behavior right after preparation. The thickness of all samples was above $l_{tot}/(2R_g) = 1.9$ to minimize the influence from confinement effects.[28−30] All observed R_c values of the PBrS samples are smaller than the ones of the PS samples, which means that brominated PS films replicated smaller in-plane length scales of the substrate roughness which may be caused by the reduced stiffness. The solid lines are fits to the data yielding $R_c \sim l_{tot}^{0.5}$.

A detailed modeling of the in-plane morphology produced right after spin-coating is very difficult due to the complex nature of the spinning process.[31,32] The process is frequently described in three consecutive phases.[1] The first phase incorporates all the initial transient effects, the second phase includes most of the mechanisms that control the resulting film thickness, and the third phase is the transition to the final film. In the second phase, the initial conditions installed at the start have been forgotten and the fluid is assumed to behave Newtonian. Viscous and centrifugal forces balance the flow, which decreases the film thickness. The viscosity depends strongly on the concentration. In the third phase, the fluid viscosity rises rapidly and further fluid loss is primarily due to solvent evaporation. The process ends when the concentration is uniform throughout the film and the viscosity is very large, preventing further flow.[1] Thus, one possible way to describe the freezing-in surface morphology is the assumption of a fluid with a strongly enhanced elastic constant. Taking the excess surface free-energy density (f^{ex}) of a liquid surface of area A that deviates from the mean height $\Delta l(\vec{\rho})$ by $h_L(\vec{\rho})$ at an in-plane position $\vec{\rho} = (x, y)$ including the bending rigidity (K)[33]

$$f^{ex}(h_L(\vec{\rho})) \approx \frac{1}{A}\int\int_A [\gamma_{LV}|\nabla h_L(\vec{\rho})|^2 + K|\nabla h_L(\vec{\rho})|^4 + P(\Delta l(\vec{\rho}))]\, d^2\rho \quad (3)$$

yields a short-wavelength cutoff.[34] Without film thickness contributions to the chemical potential difference $P(\Delta l(\vec{\rho}))$, the value of this cutoff is determined by the surface tension (γ_{LV}) and the bending rigidity

$$q_\kappa^2 = \frac{\gamma_{LV}}{K} \quad (4)$$

Using the frequently applied assumption $K_s = K/l_{tot}$, which introduces the surface elastic constant (K_s) associated with bending,[35] gives the in-plane length

$$R_c = \frac{2\pi}{q_\kappa} = 2\pi\sqrt{K_s l_{tot}/\gamma_{LV}} \sim l_{tot}^{0.5} \quad (5)$$

Thus, in a first-order estimation, R_c for a liquid film can be calculated, neglecting other nonequilibrium factors such as internal stress, spin speed, or glassiness. Within this approximation, a freezing liquid polymer solution film is expected to behave conformally for $R > R_c$. A distortion with an in-plane wavenumber $q = 2\pi/R$ decays slowly due to the small compressibility of the system in the z direction. The characteristic decay length of the distortion is given by $l(q) = 1/(\lambda q^2)$ with the material constant $\lambda = K_s/\gamma_{LV}$. From the experiment, we determine $\lambda = 7.3$ nm for PBrS and $\lambda = 13.1$ nm for PS. Thus, both values are in a comparable range with the value as determined for thin combined liquid-crystalline polymer films on silicon, $\lambda = 10.09$ nm.[36] Assuming a surface tension of PS of $\gamma_{LV} = 28.3$ mJ/m^2 [37] yields a surface elastic constant $K_s = 0.4$ nN. As expected, this value is more than 2 orders of magnitude bigger than the one of ideal simple free liquids, where K_s is negligible,[34] and bigger compared to $K_s = 0.012$ nN of free-standing smectic films.[25]

Annealing Experiments. The annealing was restricted to the PBrS samples which do not dewet on the substrates. PS samples show dewetting at long time scales; thus, a homogeneous film with a reduced interface correlation is not the equilibrium state.[4] The corresponding values of R_c for PBrS at $T = 191.8$ °C are shown as filled circles in Figure 7. The dashed line is a fit to these data yielding $R_c \sim l_{tot}^{2.0}$. Thus, we observed a crossover in the surface morphology of the polymer. During annealing, which means that the polymer is in the melt state and therefore has the freedom to relax toward equilibrium, the short-wavelength cutoff is dominated by the interaction between the substrate and the polymer molecules.[38] Assuming van der Waals interaction with an effective Hamaker constant (A_{eff})[39] yields a short-wavelength cutoff

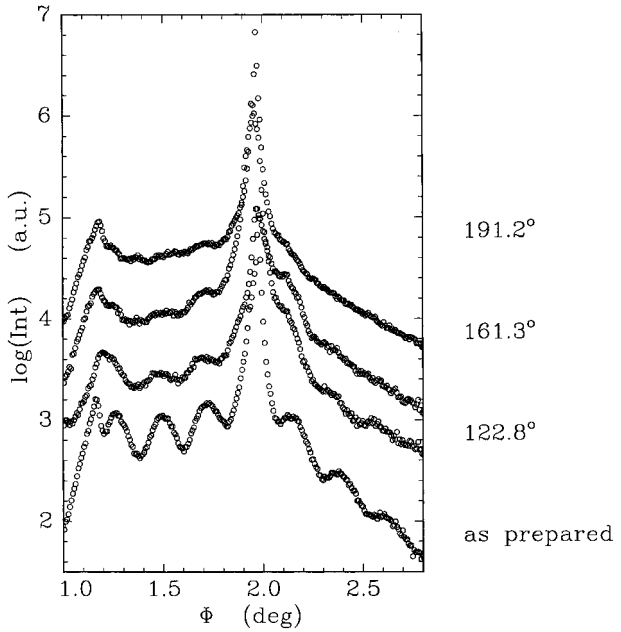

Figure 8. Detector scans measured at the angle of incidence $\alpha_i = 0.98°$ of the PBrS films with a thickness of $l_{tot} = 360$ Å as prepared and during annealing at different temperatures. For clarity, the curves are shifted by 1 order of magnitude against each other.

$$q_c^2 = \frac{1}{\gamma_{LV}}\left(\Delta\rho g + \frac{A_{eff}}{2\pi l_{tot}^4}\right) \quad (6)$$

For the investigated range of thin film thicknesses, the gravitational part ($\Delta\rho g$) can be neglected, and the result

$$R_c = \frac{2\pi}{q_c} \sim l_{tot}^{2.0} \quad (7)$$

is in accordance with the observations. The measured values of R_c are larger after annealing compared with the ones found right after preparation. Thus, only a smaller part of the roughness spectrum of the substrate is replicated in equilibrium.[40] Figure 8 shows the influence of the annealing temperature for PBrS for a film thickness of $l_{tot} = 360$ Å. After preparation, different samples were annealed at 122.8, 161.3, and 191.2 °C for more than 9 h each. The (bulk) glass-transition temperature of PBrS was determined with differential scanning calorimetry (DSC) as $T_g = 134$ °C; thermal gravimetric analysis (TGA) yields a decomposition temperature of $T_s = 415$ °C. One may take the amplitudes of the modulations of the resonant diffuse scattering as indications of the strength of the interface correlation in the annealing experiments, since the differences in the electron density remain unchanged, despite small

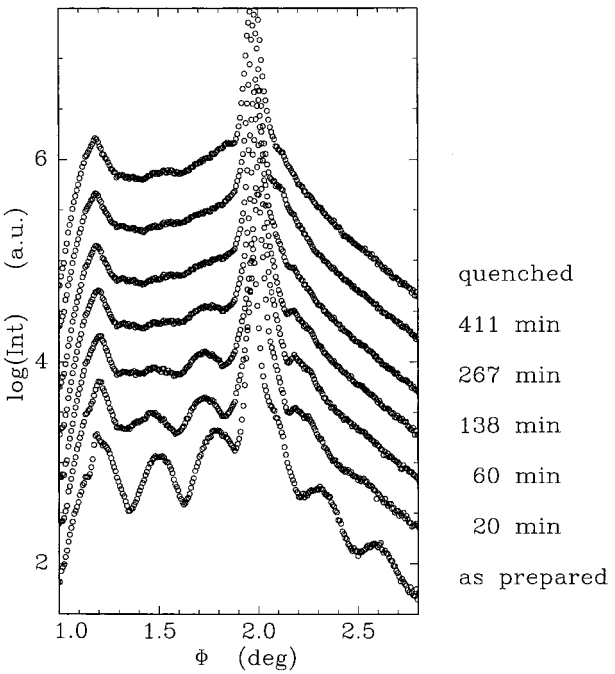

Figure 9. Detector scans measured at the angle of incidence $\alpha_i = 0.98°$ showing the time-dependent evolution of the resonant diffuse scattering of a PBrS film with a film thickness $l_{tot} = 292$ Å during annealing at $T = 191.8$ °C. For comparison, the data right after preparation (as prepared) and after a quench down to room temperature (quenched) are shown.

changes of the density due to thermal expansion. From a comparison with the unannealed sample, it is obvious that already below the glass-transition temperature a relaxation of the strongly correlated interface happened. With increasing annealing temperature, the amplitude is increasingly damped. As Figure 9 shows for a film thickness of $l_{tot} = 292$ Å at $T = 191$ °C, the equilibrium is already reached after 4.5 h. In terms of a Williams, Landel, and Ferry (WLF) approach,[41] the samples annealed at $T = 122.8$ and 161.3 °C are therefore still far from equilibrium. This explains the measured amplitudes in the detector scans shown in Figure 8, which thus represent intermediate stages of annealing. An equivalent behavior was found for other examined film thicknesses. It should be noted that at 122.8 °C, which is 11° below the bulk glass-transition temperature of PBrS, a significant decrease of roughness correlation is detected (see Figure 8). This quick relaxation was not resolvable within the limited time resolution of a synchrotron experiment, while the presented state of reduced conformality is stable over 10 h (at 122.8 °C). The changes of local heights during the relaxation are only about 1 Å perpendicular to the surface, which is very small compared to typical in-plane length scales which are larger than R_c, and displays the sensitivity of the used method. One may therefore conclude that the quick relaxation is based on a different process than chain movement like density relaxation.

In Situ Measurements. The time-dependent increase of R_c was measured in situ. The typical time resolution of the experiment was 20 min. This increased time resolution was achievable due to the enhanced scattering contrast resulting from the bromination. The determined values, normalized by the radius of gyration ($R_g = 77$ Å), are presented in the insert of Figure 10. The time $t = 0$ is defined by the start of the annealing.

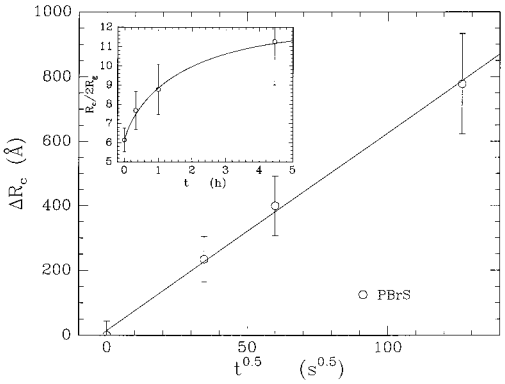

Figure 10. In situ measurement of the relaxation of the smallest replicable in-plane length scale ΔR_c as a function of the annealing time t. The annealing at $T = 191.8$ °C was started at $t = 0$. The film thickness of the PBrS sample is $l_{tot} = 292$ Å. The insert shows the time-dependent behavior of R_c normalized by the radius of gyration R_g. The solid lines are based on model calculations as explained in the text.

To extract the time constant of the observed process, we analyze the data by a mathematical model, which makes no assumptions concerning the physical origin of the measured time dependence. The solid line shows the best fit based on a Kolmogorov model (frequently called the Johnson−Mehl−Avrami model).[42−45] This model describes the time dependence of a first-order phase transformation from a metastable phase I into a stable phase II and was, for example, successfully applied to the growth of thin wetting films.[46,47] The decreasing range of R_c can be modeled if the correlated part is taken as phase I and the uncorrelated part of the roughness spectrum of the substrate as phase II, yielding a time constant $\tau = 1.8$ h. Thus, the observed relaxation is related to times well within the time regime of free diffusion.[48] The plot of the relaxed in-plane length (ΔR_c) as a function of $t^{0.5}$, shown in Figure 10, underlines that diffusion of molecules at the free surface yields the reduction of the smallest replicated in-plane length scale. Without the roughness correlation installed by the spin-coating process, both morphologies, the one of the substrate and the one of the polymer surface, would be statistically independent. The substrate morphology results from the manufacturing process of Si wafers, whereas the polymer surface in the melt state is dominated by thermally excited capillary waves. The surface tension of the polymer tries to smooth the surface; consequently, additional roughness contributions from the substrate are energetically unfavorable. Thus, the installed replicated surface roughness is a nonequilibrium state of polymer molecules, and any movement of polymer chains will lead to a reduction of roughness correlation, driven by a minimization of the surface free-energy density. Because the typical in-plane length scales are more than 2 orders of magnitude larger as compared to the amplitude of the surface roughness ($\sigma = 5$ Å), the three-dimensional movement can be reduced to a two-dimensional one. The measured diffusion in the direction of decaying concentration is described by the surface diffusion $\Delta R_c \sim (4D_s t)^{1/2}$ with a surface diffusion coefficient D_s. From the slope of Figure 10, we obtain $D_s = 9.3 \times 10^{-16}$ cm^2/s. By correlating this diffusion coefficient to the movement of molecules in the plane of the film, one can conclude that the diffusion of chains parallel to the film surface is slowed as compared to the bulk value of PS[49] ($D \cong 4$

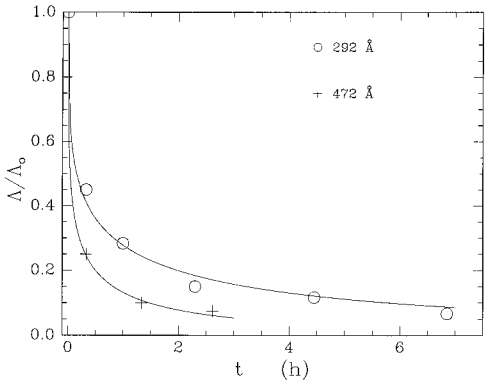

Figure 11. Time-dependent decay of roughness correlation measured in situ for two different film thicknesses of PBrS samples of l_{tot} = 292 (open circles) and 472 Å (crosses). Λ is the amplitude of the modulations in the resonant diffuse scattering, which is normalized to the value directly after preparation, Λ_0. The solid lines are fits as explained in the text.

$\times 10^{-14}$ cm^2/s). A similar slowing down was observed previously for thin PS films near an attractive interface of oxide-covered silicon up to $10R_g$ film thickness.[50,51] The values of $D \cong 1.5 \times 10^{-15}$ cm^2/s for a film thickness of about 300 Å determined for the vacuum side of the PS films[51] are in the same order of magnitude as compared to D_s. The shape of an unperturbed polymer chain in a melt or glass is well described by an ellipsoid.[52] In a bulk sample, due to the averaged random orientation, a characterization with the mean radius of gyration is possible. Computer simulations show that the presence of a hard neutral wall essentially orients the major axis of the ellipsoidal molecules parallel to the wall.[53,54] In the first approximation, the free surface of a polymer film can be regarded as a hard wall.[55] From the reduction of configurations near this wall, an enhancement of chain mobility parallel to the wall is predicted.[56,57] However, due to the strong interaction between PBrS and the substrate, the PBrS−substrate system cannot be regarded as a polymer near a neutral wall. The attractive interaction of the polymer chains and the other boundary of the polymer film, the substrate surface, decreases chain mobility by an increase of the number of contacts between the chains and the wall. Thus, on one hand, in the melt state, the in-plane diffusion is slowed down, and on the other hand, a quick relaxation is observed below the bulk glass-transition temperature. This shows the complex nature of the glass-transition phenomenon,[58] which is by far not completely understood.

To describe the decay of interface correlation, the amplitude of the modulations in the resonant diffuse scattering is examined. This yields only the relative value Λ/Λ_0 depending on the initial roughness correlation right after preparation. Figure 11 compares the time dependencies of the decaying long-range correlation for two different film thicknesses. The solid lines are fits using $\Lambda/\Lambda_0 = \exp(-(t/\tau)^{1/3})$. For the larger film thickness, the decay is faster as compared to the thinner film, which is expressed as the time constant ratio $\tau(292\ \text{Å})/\tau(472\ \text{Å}) \cong 4$. This shows that thicker films more likely lose conformality, may be due to the effect of an attractive surface. Because the examined film thicknesses (with $l_{tot}/(2R_g) > 1.9$) are larger than the typical ones showing confinement effects,[58] we observe no change in the scaling behavior and only a change in the time constant. We may conclude that regardless of the film thickness, there is an interphase region near the solid substrate where the physical properties could be very different from those in the bulk. This region could be expected to have the same extension in both examined film thicknesses, and thus, a different percentual part of the overall film thickness contributes to the film properties.

In summary, we present measurements that probe the replication of in-plane length scales from mesoscopic down to molecular in-plane distances. Roughness correlation was detected over a broad film thickness range. Thus, we investigate a collective phenomenon of many chains. At the short-wavelength cutoff, a crossover from a conformal to a statistically independent roughness spectrum is observed. For large wavelengths within the limited experimental resolution, the substrate and the polymer−vacuum interface are correlated. With spin-coating, thin polymer films with strong roughness correlation are prepared. This correlation decreases during annealing. The relaxation from the metastable, highly conformal state to the equilibrium, less conformal one was measured in situ. It yields the decay of the long-range correlation both in the strength of the correlation and the range of correlated in-plane length scales. The shorter the in-plane length scale and the thicker the polymer film, the more likely is the loss of conformality. We observe a crossover between two different types of in-plane morphologies concerning the replicated roughness. The morphology induced during the spin-coating process is dominated by bending elasticity of the freezing polymer solution, and the morphology after sufficient annealing is controlled by the van der Waals interaction between the substrate and the polymer molecules. For equilibrium, the roughness correlation of thin films is described in the framework of a linear response theory.[40] Long-wavelength fluctuations of the solid surface are followed by the liquid interface, and short-wavelength fluctuations are damped out by surface tension. With increasing film thickness, the liquid interface becomes smoother, and undulations of the solid surface are followed more closely as the film thickness decreases. With spin-coating, an unfavorable surface state was imposed in the polymer surface which relaxes T_g. The movement of the molecules at the polymer surface in the melt state is diffusion-driven in the experimentally accessible time range, yielding a surface diffusion coefficient that is small compared to the bulk diffusion coefficient. Thus, for the investigated small film thickness, we detect a long-range effect from the attractive substrate surface which slows down diffusion.

Acknowledgment. We owe many thanks to S. Cunis and G. von Krosigk for their technical assistance at the BW4 beamline, as well as to R. Gehrke for his general support of the experiment at HASYLAB. This work was supported by the DFG Schwerpunktprogramm "Benetzung und Strukturbildung an Grenzflächen" (Sta 324/8-1), and C. L. acknowledges support by a grant from the Graduiertenkolleg and J. S. G. from the GKSS Project V6.1.01.G.01-HS3.

References and Notes

(1) Lawrence, C. J. *Phys. Fluids* **1988**, *31*, 2786.
(2) Spangler, L. L.; Torkelson, M.; Royal, J. S. *Polym. Eng. Sci.* **1990**, *30*, 644.
(3) Schubert, D. W. *Polym. Bull.* **1997**, *38*, 177.
(4) Müller-Buschbaum, P.; Stamm, M. *Macromolecules* **1998**, *31*, 3686.

(5) Sinha, S. K.; Sirota, E. B.; Garoff, S.; Stanley, H. B. *Phys. Rev. B* **1988**, *38*, 2297.
(6) Daillant, J.; Bélorgey, O. *J. Chem. Phys.* **1992**, *97*, 5824.
(7) Holý, V.; Baumbach, T. *Phys. Rev. B* **1994**, *49*, 10668.
(8) Born, M.; Wolf, E. *Principles of Optics*; Pergamon: Oxford, 1964.
(9) James, R. W. *The Optical Principles of the Diffraction of X-rays*; OxBow: Woodbridge, CT, 1962.
(10) Lekner, J. *Theory of Reflection*; Martinus Nijhoff: Dodrecht, 1987.
(11) Yoneda, Y. *Phys. Rev.* **1963**, *131*, 2010.
(12) Stettner, J.; Schwalowsky, L.; Seeck, O. H.; Tolan, M.; Press: W.; Schwarz, C.; Känel, H. v. *Phys. Rev. B* **1996**, *53*, 1398.
(13) Müller-Buschbaum, P.; Vanhoorne, P.; Scheumann, V.; Stamm, M. *Europhys. Lett.* **1997**, *40*, 655.
(14) Gehrke, R. *Rev. Sci. Instrum.* **1992**, *63*, 455.
(15) Salditt, T.; Rhan, H.; Metzger, T. H.; Peisl, J.; Schuster, R.; Kotthaus, J. P. *Z. Phys. B* **1995**, *96*, 227.
(16) Müller-Buschbaum, P.; Stamm, M. *Physica B* **1998**, *248*, 229.
(17) Salditt, T.; Metzger, T. H.; Peisl, J.; Goerigk, G. *J. Phys. D: Appl. Phys.* **1995**, *28*, A236.
(18) Stearns, D. G. *J. Appl. Phys.* **1992**, *9*, 4286.
(19) Fullerton, E. E.; Pearson, J.; Sowers, J. H.; Bader, S. D.; Wu, X. Z.; Sinha, S. K. *Phys. Rev. B* **1993**, *48*, 17432.
(20) Baumbach, G. T.; Holý, V.; Pietsch, U.; Gailhanou, M. *Physica B* **1994**, *198*, 249.
(21) Schlomka, J. P.; Tolan, M.; Schwalowsky, L.; Seeck, O. H.; Stettner, J.; Press, W. *Phys. Rev. B* **1995**, *51*, 2311.
(22) Kaganer, V. M.; Stepanov, S. A.; Köhler, R. *Physica B* **1996**, *221*, 34.
(23) Gibaud, A.; Cowlam, N.; Vignaud, G.; Richardson, T. *Phys. Rev. Lett.* **1995**, *74*, 3205.
(24) Nitz, V.; Tolan, M.; Schlomka, J. P.; Seeck, O. H.; Stettner, J.; Press, W.; Stelzle, M.; Sackmann, E. *Phys. Rev. B* **1996**, *54*, 5038.
(25) Mol, E. A.; Shindler, J. D.; Shalaginov, A. N.; de Jeu, H. W. *Phys. Rev. B* **1996**, *54*, 536.
(26) Mol, E. A. L.; Wong, G. C. L.; Petit, J. M.; Rieutord, F.; de Jeu, H. W. *Phys. Rev. Lett.* **1997**, *79*, 3439.
(27) Ferry, J. D. *Viscoelastic properties of polymers*; John Wiley & Sons: New York, 1980.
(28) Reiter, G. *Europhys. Lett.* **1993**, *23*, 579.
(29) Keddie, J. L.; Jones, R. A. L.; Croy, R. A. *Europhys. Lett.* **1994**, *27*, 59.
(30) Kraus, J.; Müller-Buschbaum, P.; Bucknall, D.; Stamm, M. To be published.
(31) Emslie, A. G.; Bonner, F. T.; Peck, L. G. *J. Appl. Phys.* **1958**, *29*, 858.
(32) Bornside, D. E.; Macosko, C. W.; Scriven, L. E. *J. Electrochem. Soc.* **1991**, *138*, 317.
(33) Keller, J. B.; Merchant, G. J. *J. Stat. Phys.* **1991**, *63*, 1039.
(34) Daillant, J.; Bosio, L.; Harzallah, B.; Benattar, J. J. *J. Phys. II* **1991**, *1*, 149.
(35) Poniewierski, A.; Holyst, R. *Phys. Rev. B* **1993**, *47*, 9840.
(36) Henn, G.; Stamm, M.; Poths, H.; Rcker, M.; Rabe, J. P. *Physica B* **1996**, *221*, 174.
(37) Brandrup, J.; Kleemann, L. H. *Polymer Handbook*; Wiley & Sons: New York 1975.
(38) Dietrich, S. In *Phase Transitions and Critical Phenomena*; Domb, C., Lebowitz, J. L., Eds.; Academic: New York, 1988; Vol. 12.
(39) Lipowsky, R. *Phys. Rev. B* **1985**, *32*, 1731.
(40) Andelmann, D.; Joanny, J. F.; Robbins, M. O. *Europhys. Lett.* **1988**, *7*, 731.
(41) Tassin, J. F.; Monnerie, L.; Fetters, L. L. *Macromolecules* **1988**, *21*, 2404.
(42) Kolmogorov, A. N. *Izvestija Akad. Nank SSSR Otd. Mater. (Russ.)* **1937**, *3*, 335.
(43) Avrami, M. *J. Chem. Phys.* **1939**, *7*, 1103.
(44) Avrami, M. *J. Chem. Phys.* **1940**, *8*, 212.
(45) Avrami, M. *J. Chem. Phys.* **1941**, *9*, 177.
(46) Müller-Buschbaum, P.; Strzelczyk, M.; Tolan, M.; Press, W. *Z. Phys. B* **1995**, *98*, 89.
(47) Strzelczyk, M.; Müller-Buschbaum, P.; Tolan, M.; Press, W. *Phys. Rev. B* **1995**, *52*, 16869.
(48) Stamm, M.; Hüttenbach, S.; Reiter, G.; Springer, T. *Europhys. Lett.* **1991**, *14*, 451.
(49) Green, P. F.; Kramer, E. J. *J. Mater. Res.* **1986**, *1*, 202.
(50) Zheng, X.; Sauer, B. B.; van Alsten, J. G.; Schwarz, S. A.; Rafailovich, M. H.; Sokolov, J.; Rubinstein, M. *Phys. Rev. Lett.* **1995**, *74*, 407.
(51) Zheng, X.; Rafailovich, M. H.; Sokolov, J.; Strzhemechny, Y.; Schwarz, S. A.; Sauer, B. B.; Rubinstein, M. *Phys. Rev. Lett.* **1997**, *79*, 241.
(52) Mazur, J.; Guttman, C. M.; McCrackin, F. L. *Macromolecules* **1973**, *6*, 872.
(53) Bauschnagel, J.; Binder, K. *Macromolecules* **1995**, *28*, 6808.
(54) Pakula, T. *J. Chem. Phys.* **1991**, *95*, 4685.
(55) Wu, D. T.; Fredrickson, G. H.; Carton, J. P.; Ajdari, A.; Leibler, L. *J. Polym. Sci., Polym. Phys.* **1995**, *33*, 2373.
(56) Mansfield, K. F.; Theodorou, D. N. *Macromolecules* **1991**, *24*, 6283.
(57) Bauschnagel, J.; Binder, K. *J. Phys. I* **1996**, *6*, 1271.
(58) Forrest, J. A.; Dalnoki-Veress, K.; Dutcher, J. R. *Phys. Rev. E* **1997**, *56*, 5705.

MA981311L